

Experimental Validation of the Butyl-Rubber Finite Element (FE) Material Model for the Blast-Mitigating Floor Mat

by Masayuki Sakamoto

ARL-SR-0329

August 2015

NOTICES

Disclaimers

The findings in this report are not to be construed as an official Department of the Army position unless so designated by other authorized documents.

Citation of manufacturer's or trade names does not constitute an official endorsement or approval of the use thereof.

Destroy this report when it is no longer needed. Do not return it to the originator.

Army Research Laboratory

Adelphi, MD 20783-1138

ARL-SR-0329

August 2015

Experimental Validation of the Butyl-Rubber Finite Element (FE) Material Model for the Blast-Mitigating Floor Mat

**Masayuki Sakamoto
Japanese ESEP Research Engineer
at Weapons and Materials Research Directorate, ARL**

REPORT DOCUMENTATION PAGE				Form Approved OMB No. 0704-0188	
<p>Public reporting burden for this collection of information is estimated to average 1 hour per response, including the time for reviewing instructions, searching existing data sources, gathering and maintaining the data needed, and completing and reviewing the collection information. Send comments regarding this burden estimate or any other aspect of this collection of information, including suggestions for reducing the burden, to Department of Defense, Washington Headquarters Services, Directorate for Information Operations and Reports (0704-0188), 1215 Jefferson Davis Highway, Suite 1204, Arlington, VA 22202-4302. Respondents should be aware that notwithstanding any other provision of law, no person shall be subject to any penalty for failing to comply with a collection of information if it does not display a currently valid OMB control number.</p> <p>PLEASE DO NOT RETURN YOUR FORM TO THE ABOVE ADDRESS.</p>					
1. REPORT DATE (DD-MM-YYYY)	2. REPORT TYPE			3. DATES COVERED (From - To)	
August 2015	ESEP activity			04/2013-09/2014	
4. TITLE AND SUBTITLE				5a. CONTRACT NUMBER	
Experimental Validation of the Butyl-Rubber Finite Element (FE) Material Model for the Blast-Mitigating Floor Mat				5b. GRANT NUMBER	
				5c. PROGRAM ELEMENT NUMBER	
				5d. PROJECT NUMBER	
6. AUTHOR(S) Masayuki Sakamoto (Japanese Engineer Scientist Exchange Program Research Engineer)				5e. TASK NUMBER	
				5f. WORK UNIT NUMBER	
7. PERFORMING ORGANIZATION NAME(S) AND ADDRESS(ES) US Army Research Laboratory ATTN: RDRL-WMP-F 2800 Powder Mill Road Adelphi, MD 20783-1138				8. PERFORMING ORGANIZATION REPORT NUMBER	
				ARL-SR-0329	
9. SPONSORING/MONITORING AGENCY NAME(S) AND ADDRESS(ES) Survivability and Firepower Analysis Section, Ballistic Research Division, Ground Systems Research Center ATTN: Masayuki Sakamoto 2-9-54, Fuchinobe, Chuo-ku, Sagamihara-shi, Kanagawa-ken 252-0206, JAPAN				10. SPONSOR/MONITOR'S ACRONYM(S)	
				11. SPONSOR/MONITOR'S REPORT NUMBER(S)	
12. DISTRIBUTION/AVAILABILITY STATEMENT Approved for public release; distribution unlimited.					
13. SUPPLEMENTARY NOTES Engineer Scientist Exchange Program between US and Japan Because one of the authors of this report is an employee of the Japanese Ministry of Defense (JMOD), this report cannot be published without approval by the appropriate Japanese organization. At the completion of the formal review process, and before publication, please forward this report to the Technical Research and Development Institute (TRDI), JMOD for approval to publish this report (JMOD/TRDI POC: Mr. Masayuki Sakamoto, Survivability and Firepower Analysis Section, Ballistic Research Division, Ground Systems Research Center [E-mail: masayuki@cs.trdi.mod.go.jp , Phone: +81-42-752-2941, Address: 2-9-54, Fuchinobe, Chuo-ku, Sagamihara-shi, Kanagawa-ken 252-0206, JAPAN]). Retain a copy of the approval with the Form-1 record.					
14. ABSTRACT This report was written by the author under the Engineer Scientist Exchange Program activity in the US Army Research Laboratory from April 2013 to September 2014. To clarify the accuracy of finite element (FE) material models for butyl rubber, the component-level loading test was conducted on drop testers in various loading conditions. The test results are compared with the Finite Element Analysis (FEA) results of each FE-material model, and the errors in each material model are discussed on various metrics.					
15. SUBJECT TERMS ESEP, Blast-mitigating floor mat, Viscoelastic material, LS-DYNA					
16. SECURITY CLASSIFICATION OF:			17. LIMITATION OF ABSTRACT	18. NUMBER OF PAGES	19a. NAME OF RESPONSIBLE PERSON Robert G Kargus
a. REPORT Unclassified	b. ABSTRACT Unclassified	c. THIS PAGE Unclassified	UU	36	19b. TELEPHONE NUMBER (Include area code) (301) 394-5738

Contents

List of Figures	iv
List of Tables	v
Acknowledgments	vi
1. Introduction	1
2. Experiment and Analysis Methods	1
2.1 Butyl Rubber.....	1
2.2 Component Loading Test.....	2
2.3 Measurement.....	4
2.4 Finite Element Analysis	6
3. Results and Discussion	11
3.1 Experimental Results.....	11
3.2 Comparison in Stress and Strain Histories.....	14
3.3 Comparison in Stress–Strain Curves	18
4. Conclusions	24
5. References and Notes	25
6. List of Symbols, Abbreviations, and Acronyms	26
Distribution List	27

List of Figures

Fig. 1	Test specimen of the butyl rubber	2
Fig. 2	Front view of the finger-crusher test rig on the loading table of the drop tester equipped with a specimen and sensors.....	2
Fig. 3	Dimensions of the finger-crusher test rig.....	3
Fig. 4	Arrangements of sensors in the test setup.....	5
Fig. 5	FE model of the component loading test	6
Fig. 6	Strain-rate-dependent loading–unloading curves for the ARL model	9
Fig. 7	Schematic of boundary conditions in FEAs	9
Fig. 8	Velocity histories on the loading table in FEAs for 4-millisecond (msec) pulse loading.....	10
Fig. 9	Velocity histories on the loading table in FEAs for 8-msec-pulse loading	10
Fig. 10	Velocity histories on the loading table in FEAs for 20-msec-pulse loading	11
Fig. 11	Typical load and deformation histories of the component loading test, X08_30_03 ($\Delta T = 8$ msec, $\Delta V = 3.0$ meters per second [m/s])	12
Fig. 12	Example of the engineering stress history comparison between experiments and FEAs, X04_60 ($\Delta T = 4$ msec, $\Delta V = 6.0$ m/s)	14
Fig. 13	Example of the engineering stress history comparison between experiments and FEAs, X08_60 ($\Delta T = 8$ msec, $\Delta V = 6.0$ m/s)	15
Fig. 14	Example of the engineering stress history comparison between experiments and FEAs, X20_60 ($\Delta T = 20$ msec, $\Delta V = 6.0$ m/s)	15
Fig. 15	Example of the engineering strain history comparison between experiments and FEAs, X04_60 ($\Delta T = 4$ msec, $\Delta V = 6.0$ m/s)	16
Fig. 16	Example of the engineering strain history comparison between experiments and FEAs, X08_60 ($\Delta T = 8$ msec, $\Delta V = 6.0$ m/s)	16
Fig. 17	Example of the engineering strain history comparison between experiments and FEAs, X20_60 ($\Delta T = 20$ msec, $\Delta V = 6.0$ m/s)	17
Fig. 18	Peak stress errors of FEAs vs. experimental test data.....	18
Fig. 19	Impulse per unit cross-section errors of FEAs vs. experimental test data	18
Fig. 20	Peak strain errors of FEAs vs. experimental test data.....	18
Fig. 21	Example of the engineering stress–strain curve comparison between experiments and FEAs, X04_60 ($\Delta T = 4$ msec, $\Delta V = 6.0$ m/s)	19
Fig. 22	Example of the engineering stress–strain curve comparison between experiments and FEAs, X08_60 ($\Delta T = 8$ msec, $\Delta V = 6.0$ m/s)	19

Fig. 23	Example of the engineering stress-strain curve comparison between experiments and FEAs, X20_60 ($\Delta T = 20$ msec, $\Delta V = 6.0$ m/s).....	20
Fig. 24	Schematic of the stress-strain curve and metrics	21
Fig. 25	Initial modulus errors of FEAs versus experimental test data.....	22
Fig. 26	Loading modulus errors of FEAs versus experimental test data.....	22
Fig. 27	Encircled area errors of FEAs versus experimental data. (LSTC model's errors are omitted due to poor differentiation in the loading-unloading curves.).....	22
Fig. 28	Strain-rate histories of the specimen in the test condition, X04_60 ($\Delta T = 4$ msec, $\Delta V = 6.0$ m/s).....	23

List of Tables

Table 1	Loading conditions for the component loading test	4
Table 2	Specifications of sensors used in the component loading test.....	5
Table 3	FE-material models for the test rig's parts.....	6
Table 4	FE-material models for the butyl-rubber specimen part	7
Table 5	LS-DYNA material card for the LSTC model	7
Table 6	LS-DYNA material card for the Humanetics model.....	8
Table 7	LS-DYNA material card for the ARL model	8
Table 8	Summary of experimental results	13

Acknowledgments

This report was written by the author under the Engineer Scientist Exchange Program activity in the US Army Research Laboratory (ARL) from April 2013 to September 2014. I would like to take this opportunity to thank the ARL for giving me the chance to learn and investigate blast-loading issues in the state-of-the-art research environment. I also would like to thank the members of the Blast Protection Branch and its specialists for supporting the numerical analysis, experiment, data processing, and various discussions that gave me valuable ideas.

1. Introduction

Lower leg injury is a major injury mode induced by underbody blast loading associated with improvised explosive device (IED) attacks against ground fighting vehicles.¹⁻⁴ Blast-mitigating floor mats are regarded as an effective countermeasure for injury prevention,^{5,6} and the methodology for their selection and optimization is in immediate need. However, the loading mechanics in the lower leg with the existence of the floor mat are not fully understood. Thus, we decided to clarify the mechanics through the Finite Element Analysis (FEA). In this approach, we selected the combination of the Hybrid III 50th Percentile anthropomorphic test device's (ATD's) lower leg and the butyl-rubber floor mat with their well-known characteristics.

There are several finite element (FE) material models for the butyl rubber, and it is necessary to determine which model is to be used in the FEA. In this report, we present the accuracy of FE-material models for the butyl rubber through the comparison between the FEA and component loading test.

2. Experiment and Analysis Methods

2.1 Butyl Rubber

The butyl rubber used in this study was manufactured by Humanetics Innovative Solutions. This is the same material used in the neck components of the Hybrid III 50th Percentile ATD. The dimensions of a bulk sheet were 8 inches \times 8 inches \times 20 millimeters (mm), and test specimens were cut off from the sheet in the shape of cylinders (ϕ 3 inches \times 20 mm) as shown in Fig. 1. Before the component loading test was conducted, each specimen received compression loading up to 40% deformation against its thickness. This preloading process was intended to initialize the material status considering the Mullins effect, and neither permanent deformation nor fracture occurred on the specimens during this process.



Fig. 1 Test specimen of the butyl rubber

2.2 Component Loading Test

The component loading test was conducted on the drop tester with the finger-crusher test rig in Fig. 2. The dimensions of the test rig are shown in Fig. 3. In this test setup, the lower plate, load cell, and base were rigidly assembled and fixed on the loading table of the drop tester. Thus, the specimen was compressed between the plates in the drop impact, and the material's behavior was known from the applied load and displacement between the plates.

The test was conducted on the drop testers (Lansmont, P65 and P45) at the Adelphi Laboratory Center, U.S. Army Research Laboratory (ARL), at room temperature. The loading conditions in the test are listed in Table 1. Test specimens were reused several times after the confirmation of the material's condition, and the interval between each test was kept to more than an hour for the material's relaxation.

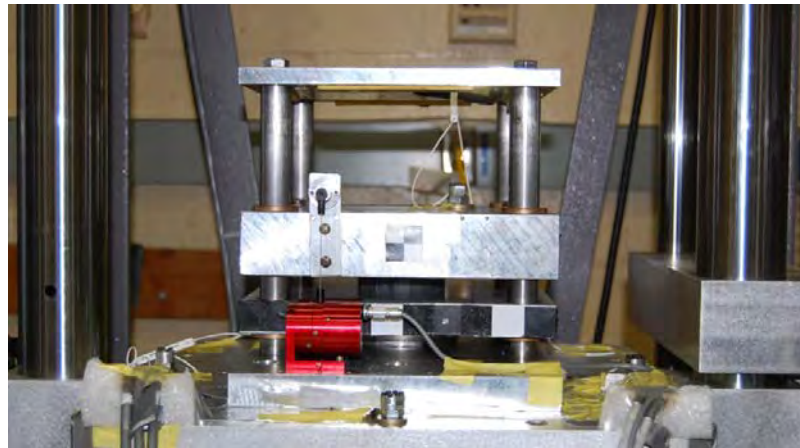


Fig. 2 Front view of the finger-crusher test rig on the loading table of the drop tester equipped with a specimen and sensors

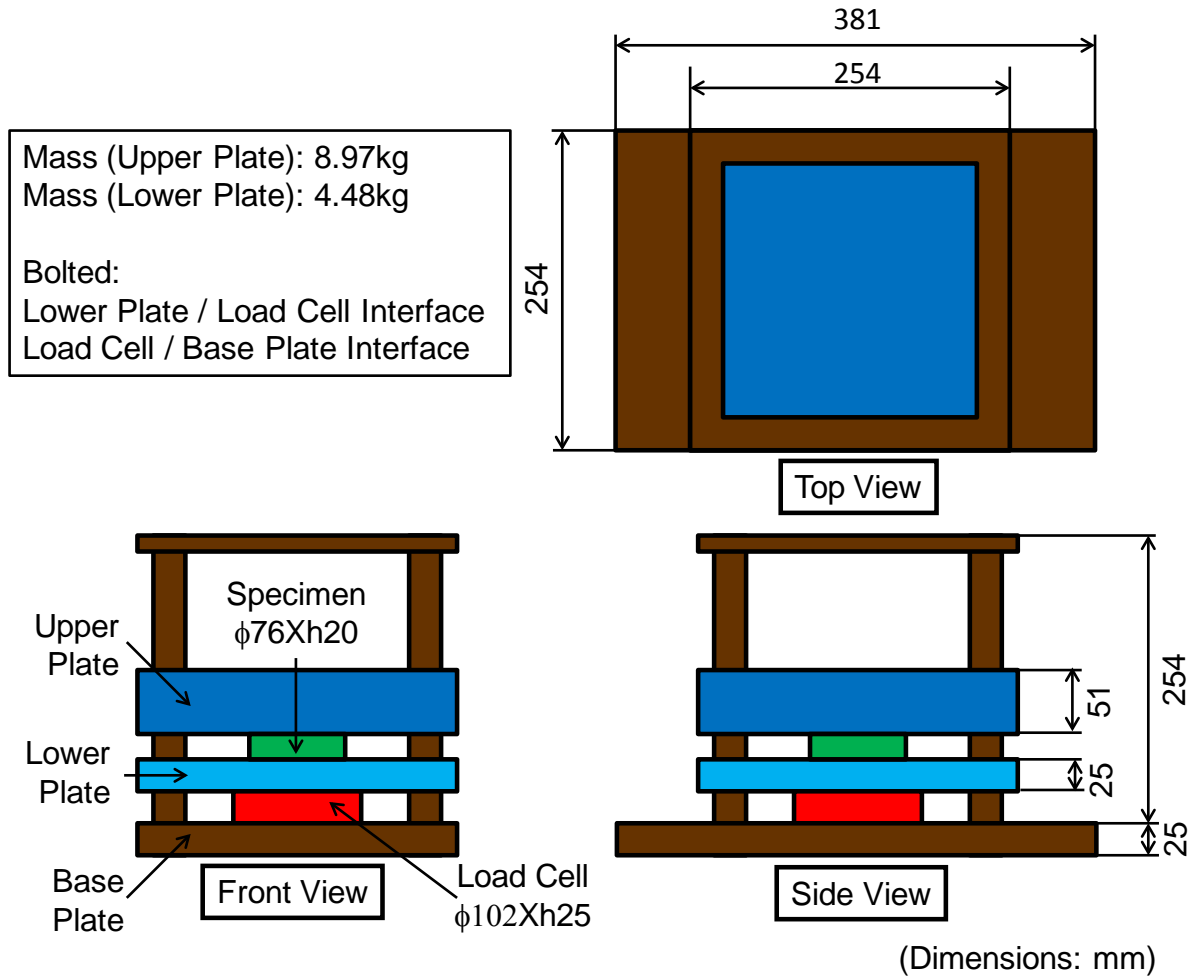


Fig. 3 Dimensions of the finger-crusher test rig

Table 1 Loading conditions for the component loading test

Pulse Duration, ΔT (msec)	Velocity Change on the Loading Table, ΔV (m/s)	Condition Code
4	Velocity	3.0
		4.5
		6.0
8		3.0
		4.5
		6.0
20		3.0
		4.5
		6.0

2.3 Measurement

The arrangements of sensors in the test setup are shown in Fig. 4, and the specifications are listed in Table 2. The signals from sensors were recorded in the data acquisition system (Spectral Dynamics, SYSCHASVXI-5) at the sampling frequency of 250 kHz. Moreover, direct-current offset and a CFC1000 filter were applied to each signal in the postprocessing on the data-analysis software (MathWorks, MATLAB). The test was also recorded by the high-speed imaging camera (Phantom, Miro) for the confirmation of the specimen's behavior and the test rig's rigidity.

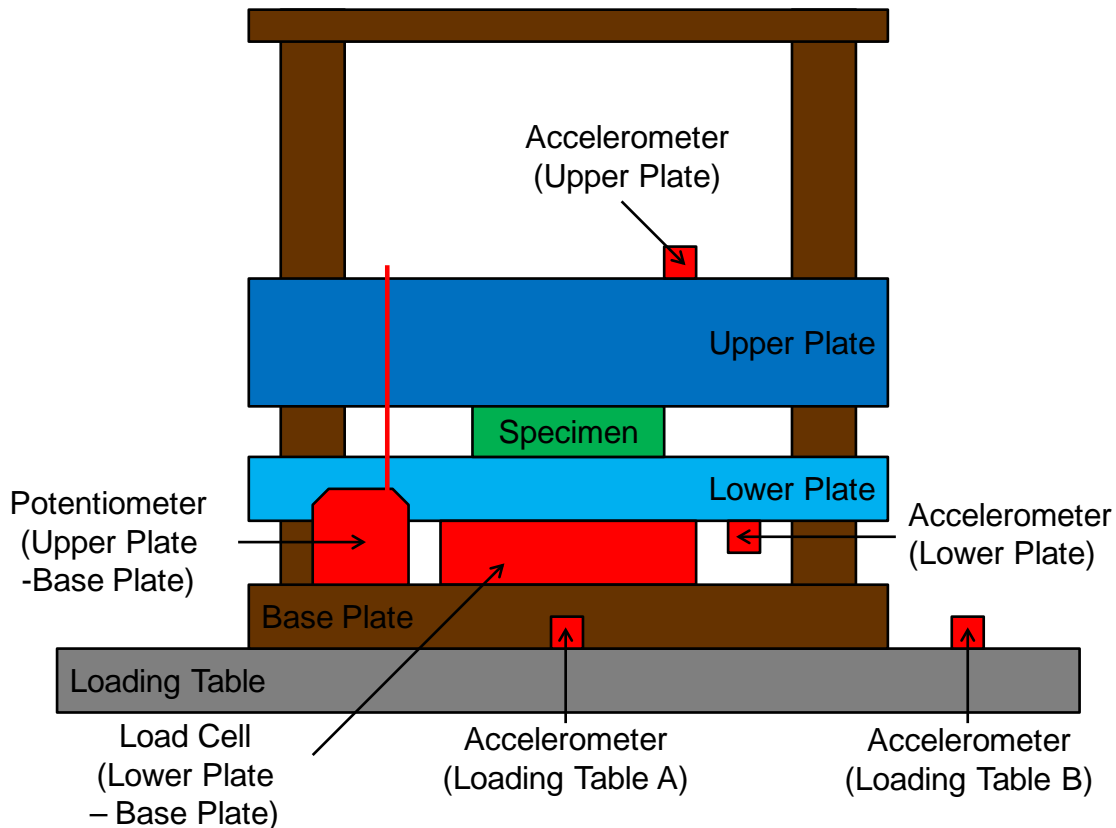


Fig. 4 Arrangements of sensors in the test setup

Table 2 Specifications of sensors used in the component loading test

Sensor	Position	Type	Range
Accelerometer	Loading TableA	Endevco 7270A-20KM6	20000G
	Loading TableB		
Accelerometer	Upper Plate	Endevco 7270A-60KM6	60000G
	Lower Plate		
Load cell	Lower Plate - Base Plate	Omegadyne LC8400-213	10000lbf
Potentiometer	Upper Plate - Base Plate	Celesco MT2A-30E-33	30in.

The input acceleration used to calculate ΔV on the loading table was the average of the outputs from 2 accelerometers (Loading Tables A and B). The load applied on the specimen L_m was calculated from the output from the load cell L considering the inertial effect of the lower plate, as follows:

$$L_m = L - m_l \times a_l, \quad (1)$$

where m_l is the lower plate's mass, and a_l is the acceleration on the lower plate.

2.4 Finite Element Analysis

There are 3 FE-material models for the butyl rubber fabricated on LS-DYNA simulation software by different developers: Livermore Software Technology Corp. (LSTC), Humanetics, and the ARL. In this study, we evaluated the accuracy of these models by comparing their FEA results with those of experiments with the finger-crusher test rig. Therefore, the FE model of the component loading test was built on LS-DYNA (Fig. 5) using material models listed in Table 3 for the test rig's parts.

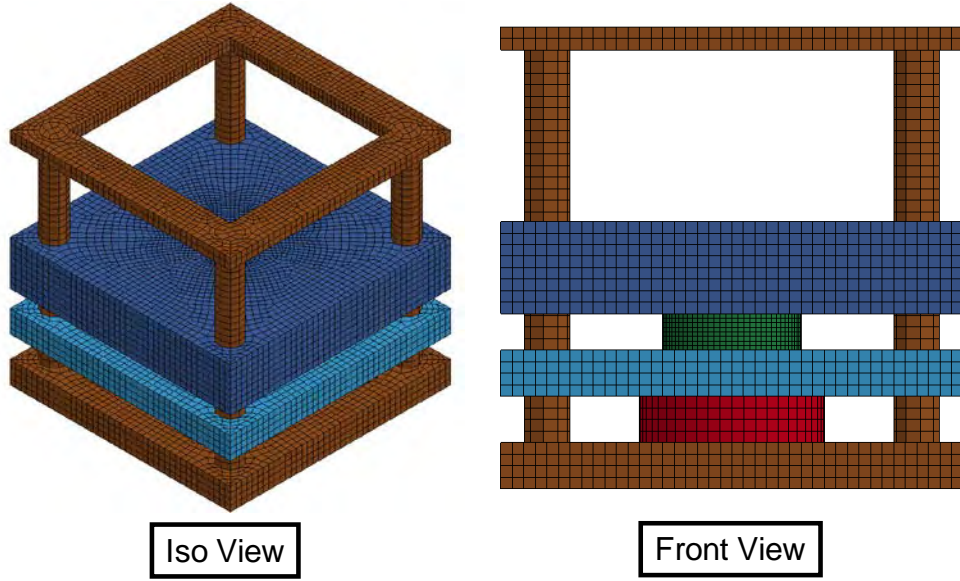


Fig. 5 FE model of the component loading test

Table 3 FE-material models for the test rig's parts

Part	Material	Model Type in LS-DYNA	Parameters
Frame			
Upper Plate	Aluminum	MAT_020_ RIGID	RO=2.816e-6 (kg/mm ³) E=70 (GPa)
Lower Plate			PR=0.30
Load Cell	Stainless Steel	MAT_020_ RIGID	RO=8.000e-6 (kg/mm ³) E=193 (GPa) PR=0.30

Three FE material models listed in Table 4 were used for the specimen part to make corresponding FE models. The LSTC material model and Humanetics material model are derived from the neck component of the Hybrid III 50th ATD FEA models developed by LSTC and Humanetics.^{7,8} Both models are derivative of a viscoelastic material model, and the LSTC model is the most simplified description.⁹ In addition to viscoelasticity, the Humanetics model contains Ogden hyperelasticity for the equilibrium part.¹⁰

Table 4 FE-material models for the butyl-rubber specimen part

Developer	Model Type in LS-DYNA	Model Description
LSTC	MAT_006_VISCOELASTIC	Linear Viscoelastic Model
Humanetics	MAT_0770_OGDEN_RUBBER	Ogden Hyperelastic Rubber Model with Viscoelasticity (First-Order Prony Function)
ARL	MAT_183_SIMPLIFIED_RUBBER_WITH_DAMAGE	Incompressible Rubber Model with Strain-Rate Dependent Loading / Unloading Curves

The LS-DYNA material cards used for the LSTC and Humanetics models are listed in Tables 5 and 6. By contrast, the ARL model is a form-type model and refers to loading–unloading curves for its response considering strain-rate dependency.¹¹ The material card of the ARL model is listed in Table 7.

Table 5 LS-DYNA material card for the LSTC model

Parameters
RO=1.1000e-6 (kg/mm ³)
BULK=0.1128 (GPa)
G0=0.0046 (GPa)
GI=0.0010 (GPa)
BETA=0.11000

Table 6 LS-DYNA material card for the Humanetics model

Parameters
RO=1.700e-6 (kg/mm ³)
PR=0.49
MU1=8.100e-004 (GPa)
MU2=7.220e-005 (GPa)
MU3=-9.710e-005 (GPa)
ALPHA1=1.3
ALPHA2=4.0
ALPHA3=-2.0
GI=3.200E-2 (GPa)
BETA1=1.600 (GPa)

Table 7 LS-DYNA material card for the ARL model

Parameters
RO=1.600e-6 (kg/mm ³)
K=2.900 (GPa)
MU=0.900 (GPa)
G=0.100 (GPa)
SIGF=1.000e-4 (GPa)

The ARL model's loading–unloading curves are developed through the dynamic loading test developed at Purdue University as shown in Fig. 6.

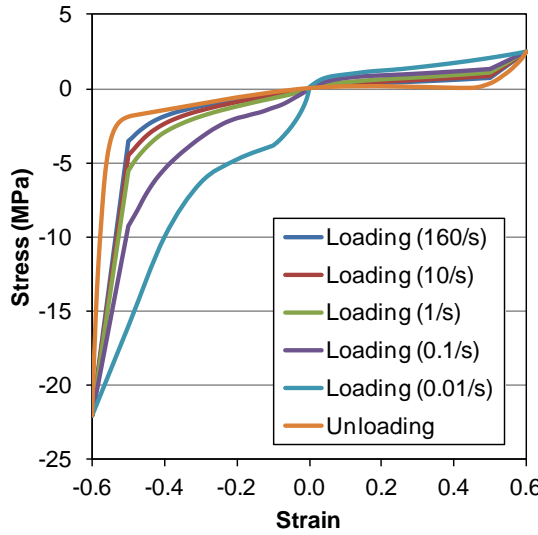


Fig. 6 Strain-rate-dependent loading-unloading curves for the ARL model

Each FE model was applied the same boundary conditions as shown in Fig. 7 according to the acceleration histories on the loading table in experiments. Thus, the velocity histories in Fig. 8–10 were generated on FE models as the loading conditions.

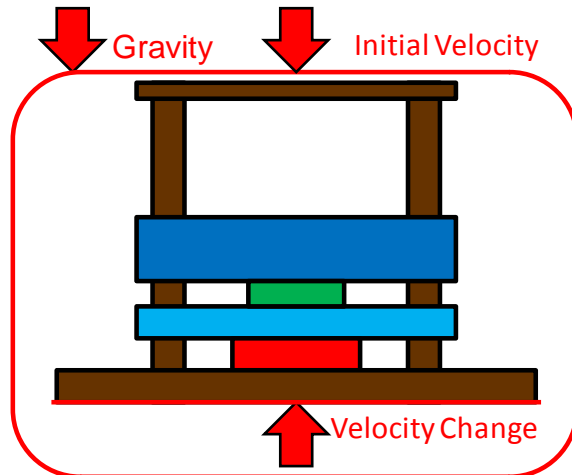


Fig. 7 Schematic of boundary conditions in FEAs

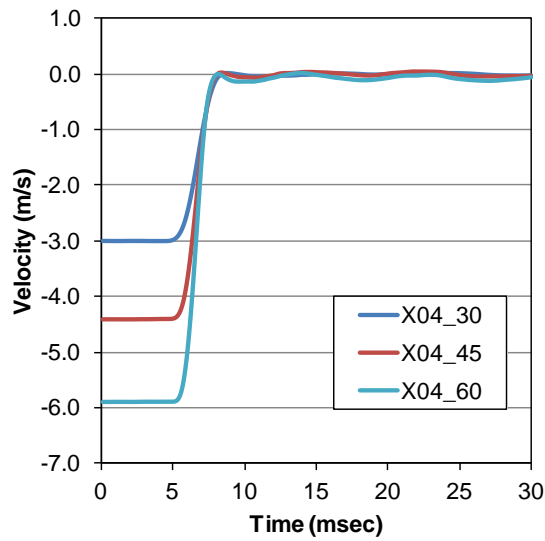


Fig. 8 Velocity histories on the loading table in FEAs for 4-millisecond (msec) pulse loading

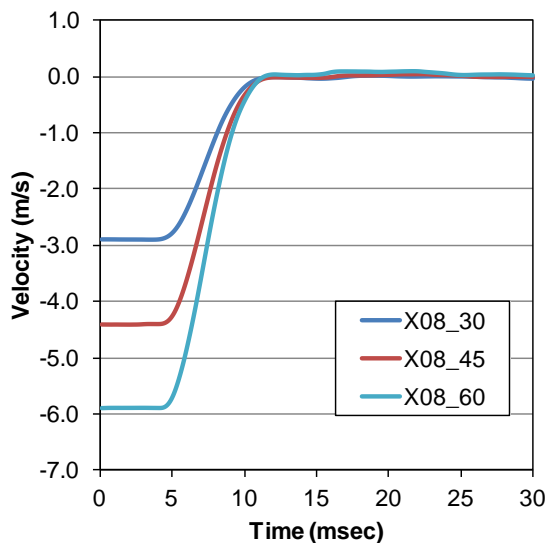


Fig. 9 Velocity histories on the loading table in FEAs for 8-msec-pulse loading

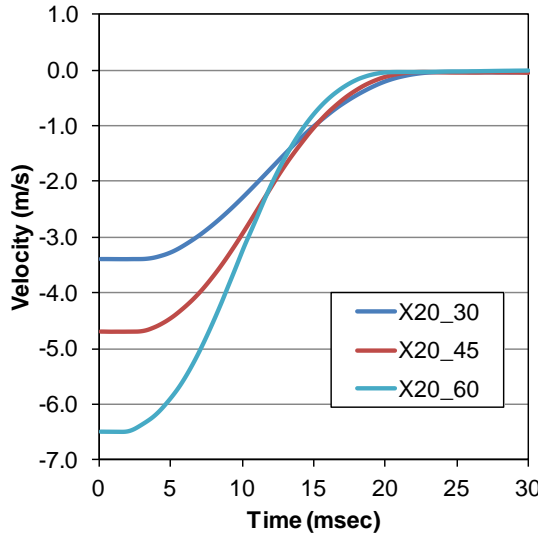


Fig. 10 Velocity histories on the loading table in FEAs for 20-msec-pulse loading

3. Results and Discussion

3.1 Experimental Results

Typical load and deformation histories of the component loading test are shown in Fig. 11. There is a delay in the deformation response most likely due to the viscoelastic behavior of the butyl rubber. The experimental results are summarized in Table 8.

The deviation of the results in each loading condition is less than 10% except for the deformation peak in 20-msec-pulse loading, and these are believed to be small enough to compare the results with those of FEAs. Considering the accuracy of the potentiometer (Celesco MT2A-30E-33, 0.15% of full scale), it seems that the small deformations in 20-msec-pulse loading were not measured precisely. Therefore, the reliability of these results is lower than that of others. This should be considered in the following discussion.

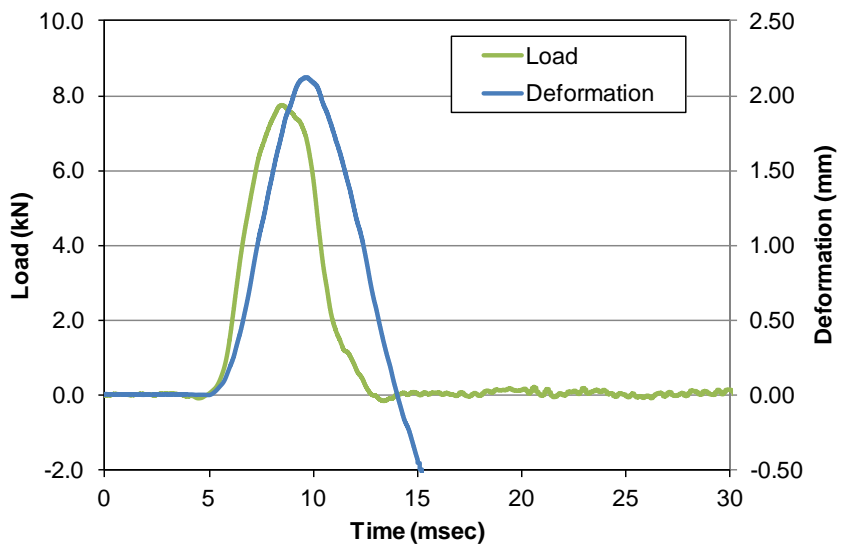


Fig. 11 Typical load and deformation histories of the component loading test, X08_30_03 ($\Delta T = 8$ msec, $\Delta V = 3.0$ meters per second [m/s])

Table 8 Summary of experimental results

Shot Code	Pulse Duration, ΔT (msec)	Table Velocity Change, ΔV (m/s)	Loading	Peak Load (kN)	Applied Impulse (kN msec)	Peak Deformation (mm)
X04_30_01	4.7	3.0		13.3	31.1	3.36
X04_30_02	4.5	3.0		13.9	32.1	3.25
X04_30_03	4.2	3.0		13.4	31.7	3.14
Avg. / SD	4.5 / 6%	3.0 / 0%		13.5 / 2%	31.6 / 2%	3.25 / 3%
X04_45_01	3.9	4.4		22.7	47.3	4.87
X04_45_02	3.7	4.4		23.6	47.6	4.92
X04_45_03	3.9	4.4		22.6	46.3	5.09
Avg. / SD	3.8 / 3%	4.4 / 0%		23.0 / 2%	47.1 / 1%	4.96 / 2%
X04_60_01	3.3	6.0		35.3	62.4	5.73
X04_60_02	3.3	5.9		36.2	62.7	6.22
X04_60_03	3.2	5.9		35.9	63.2	6.28
Avg. / SD	3.3 / 2%	5.9 / 1%		35.8 / 1%	62.8 / 1%	6.08 / 5%
X08_30_01	8.3	2.9		7.4	29.7	1.73
X08_30_02	8.5	2.8		7.2	30.6	1.93
X08_30_03	9.0	3.0		7.7	30.4	2.12
Avg. / SD	8.6 / 4%	2.9 / 3%		7.5 / 3%	30.2 / 2%	1.93 / 9%
X08_45_01	8.4	4.4		11.3	45.0	2.77
X08_45_02	8.6	4.4		11.1	44.3	2.85
X08_45_03	8.0	4.4		11.2	44.7	2.66
Avg. / SD	8.3 / 4%	4.4 / 0%		11.2 / 1%	44.7 / 1%	2.76 / 3%
X08_60_01	7.9	5.9		16.1	59.4	4.01
X08_60_02	8.0	5.9		15.5	58.6	3.97
X08_60_03	8.0	6.0		16.1	59.2	3.74
Avg. / SD	8.0 / 1%	5.9 / 1%		15.9 / 2%	59.0 / 1%	3.91 / 4%
X20_30_01	21.9	3.5		2.6	32.3	0.79
X20_30_02	21.7	3.3		2.6	32.3	0.63
X20_30_03	21.5	3.3		2.5	30.0	0.64
Avg. / SD	21.7 / 1%	3.4 / 3%		2.6 / 2%	31.5 / 4%	0.69 / 13%
X20_45_01	20.7	4.6		4.1	44.2	0.62
X20_45_02	19.9	4.7		4.1	45.8	0.60
X20_45_03	21.2	4.8		4.2	45.4	1.26
Avg. / SD	20.6 / 3%	4.7 / 2%		4.1 / 1%	45.1 / 2%	0.83 / 45%
X20_60_01	19.9	6.5		6.4	62.0	1.77
X20_60_02	19.3	6.6		6.8	61.6	1.81
X20_60_03	19.0	6.5		6.2	60.6	2.03
Avg. / SD	19.4 / 2%	6.5 / 1%		6.5 / 5%	61.4 / 1%	1.87 / 7%

3.2 Comparison in Stress and Strain Histories

The load and deformation histories of each experiment were transferred to the engineering stress and engineering strain histories according to the measured dimensions of the specimen. The stress and strain histories are shown in Figs. 12–17 with corresponding FEA results of each material model. The FEA results of the Humanetics model and ARL model agree with the experimental results in most of the loading conditions including delays in strain histories.

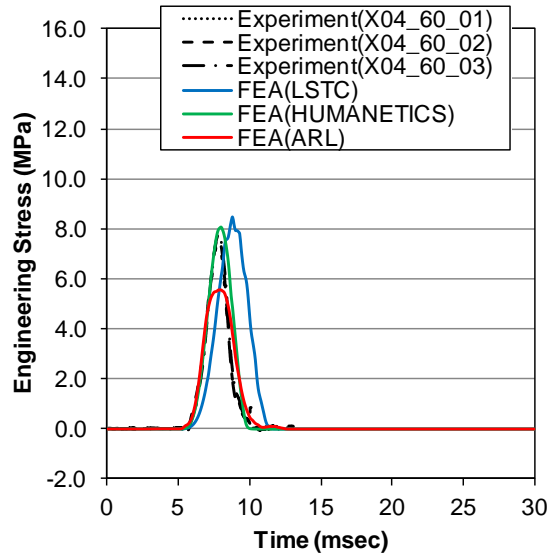


Fig. 12 Example of the engineering stress history comparison between experiments and FEAs, X04_60 ($\Delta T = 4$ msec, $\Delta V = 6.0$ m/s)

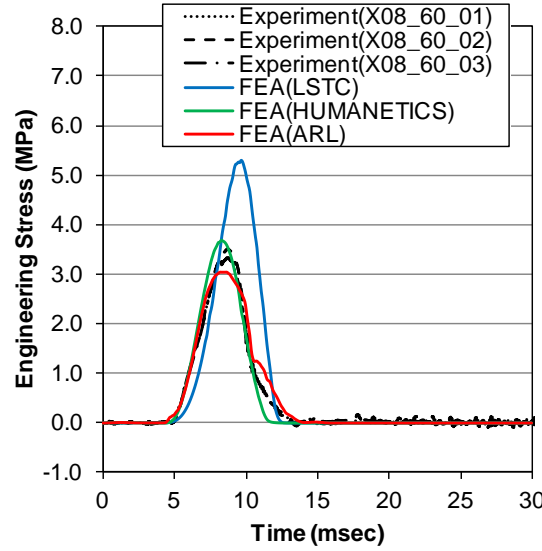


Fig. 13 Example of the engineering stress history comparison between experiments and FEAs, X08_60 ($\Delta T = 8$ msec, $\Delta V = 6.0$ m/s)

However, the FEA results of the LSTC model significantly overshoot the experimental results in several loading conditions. Moreover, the LSTC model shows unrealistic double-curved response in 20-msec-pulse loading as shown in Fig. 14 and 17.

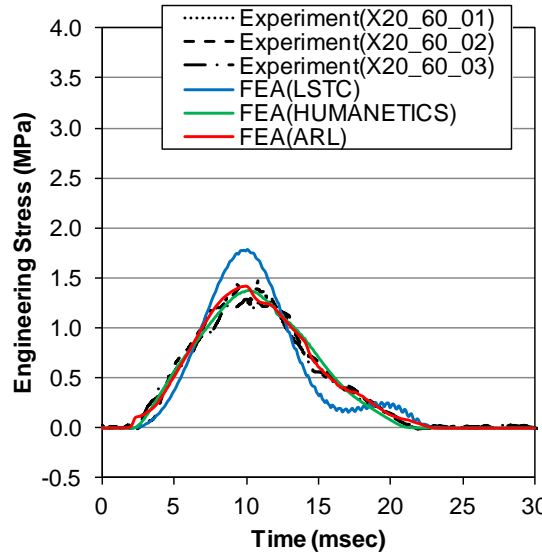


Fig. 14 Example of the engineering stress history comparison between experiments and FEAs, X20_60 ($\Delta T = 20$ msec, $\Delta V = 6.0$ m/s)

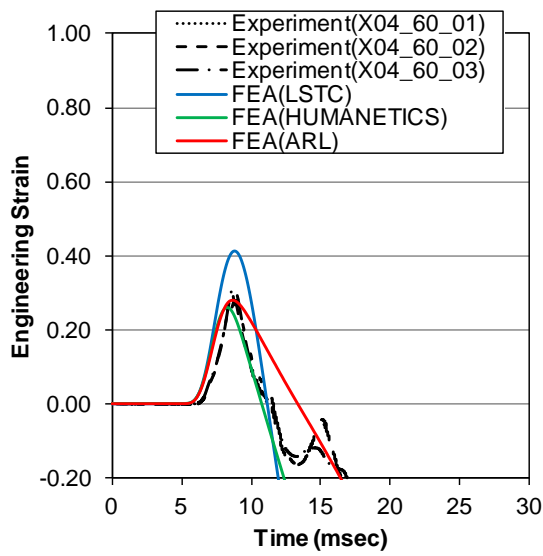


Fig. 15 Example of the engineering strain history comparison between experiments and FEAs, X04_60
 $(\Delta T = 4 \text{ msec}, \Delta V = 6.0 \text{ m/s})$

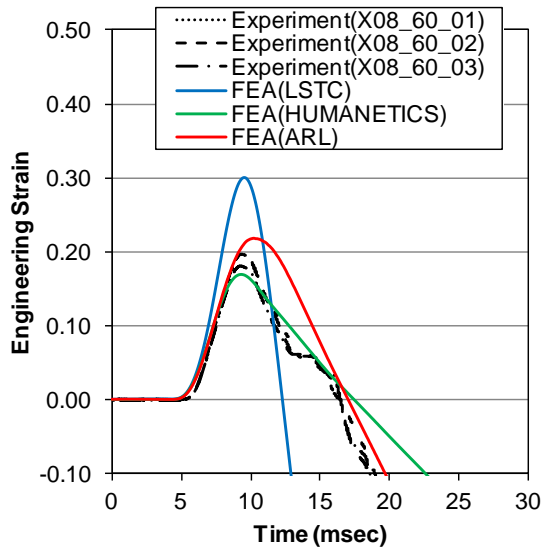


Fig. 16 Example of the engineering strain history comparison between experiments and FEAs, X08_60
 $(\Delta T = 8 \text{ msec}, \Delta V = 6.0 \text{ m/s})$

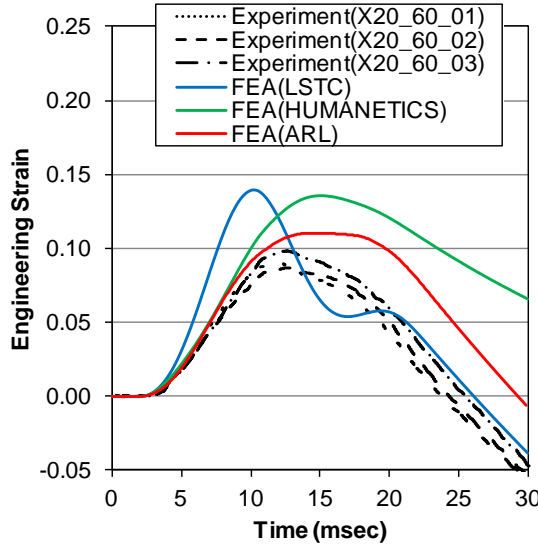


Fig. 17 Example of the engineering strain history comparison between experiments and FEAs, X20_60 ($\Delta T = 20$ msec, $\Delta V = 6.0$ m/s)

To clarify the accuracy of each material model, the errors of the FEA results versus the experimental results were compared for the peak stress, impulse per unit cross-section, and peak strain in Figs. 18–20. Thus, the errors probably have some relationships with the pulse durations because the tendencies are similar among loading conditions with the same pulse duration. Therefore, we will discuss the accuracy of material models mainly from this point of view.

The errors of the Humanetics model and the ARL model are less than 25% except for the strain errors in 20-msec-pulse loading, although the LSTC model has considerably larger errors. The strain errors in 20-msec-pulse loading are still large after considering the low reliability of the deformation measurement; the deviation in strain histories in the unloading phase of 20-msec-pulse loading is also large (Fig. 17). Because of the characteristic of viscoelastic material models, the Humanetics model assumes the same behavior for the loading–unloading phases; the ARL model considers only one curve for the unloading phase regardless of strain rate (as was shown in Fig. 6). Consequently, the unloading phases of each model contain larger errors than those of the loading phases (Fig. 20). Together with the long pulse duration, this probably leads to the accumulation of strain errors in 20-msec-pulse loading.

For these reasons, both the Humanetics model and ARL model can be used for the prediction of stress and strain histories, and also for that of impulse transfer in 4- and 8-msec-pulse loading. However, they require cautious use in longer-duration pulse loading.

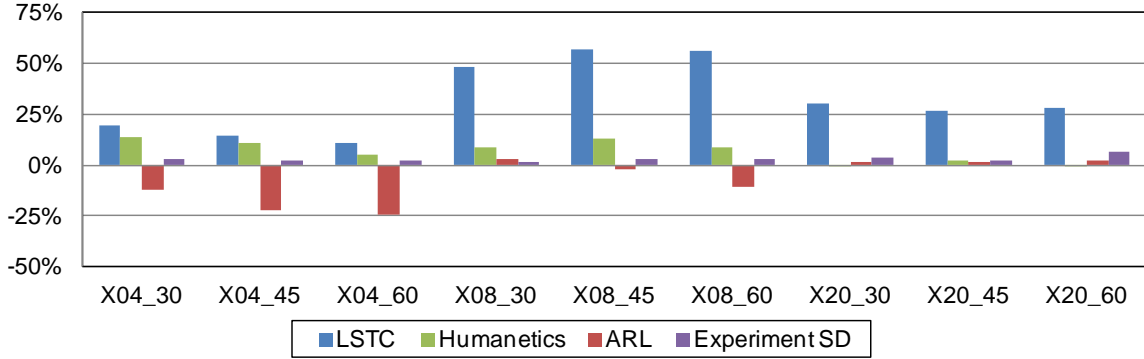


Fig. 18 Peak stress errors of FEA models vs. experimental test data

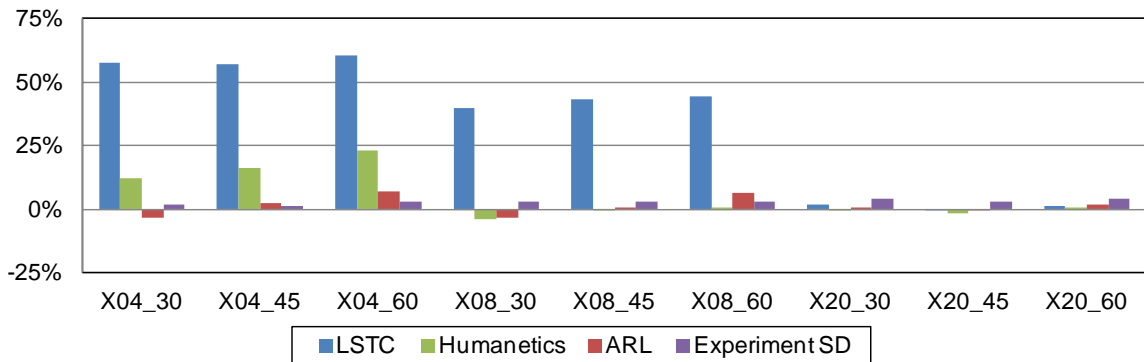


Fig. 19 Impulse per unit cross-section errors of FEA models vs. experimental test data

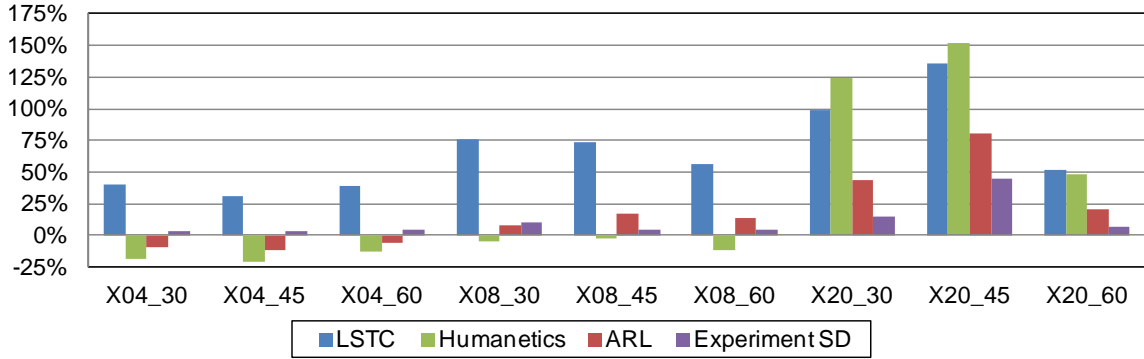


Fig. 20 Peak strain errors of FEA models vs. experimental test data

3.3 Comparison in Stress–Strain Curves

The stress and strain histories of each experiment were combined into stress–strain curves. The curves are shown in Figs. 21–23 with corresponding FEA results of each material model. The stress–strain curves in the experimental results show different paths for the loading–unloading phases and form encircled areas. The FEA results of the Humanetics model and ARL model agree with the experimental results in the formation of these encircled areas. By contrast, the

FEA results of the LSTC model show almost identical paths for the loading–unloading phases in 4- and 8-msec-pulse loading, as shown in Figs. 21 and 22.

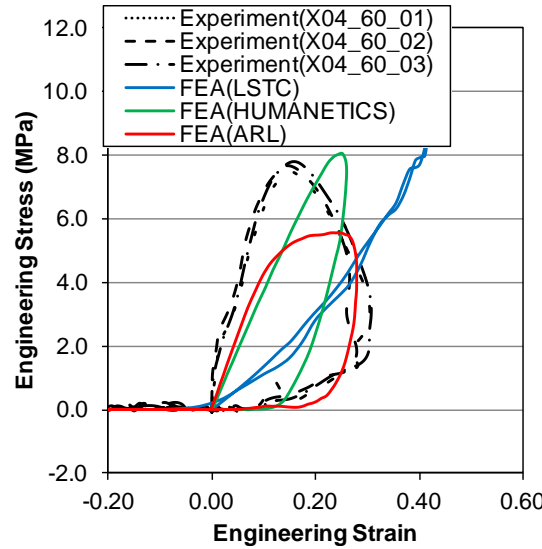


Fig. 21 Example of the engineering stress–strain curve comparison between experiments and FEAs, X04_60 ($\Delta T = 4$ msec, $\Delta V = 6.0$ m/s)

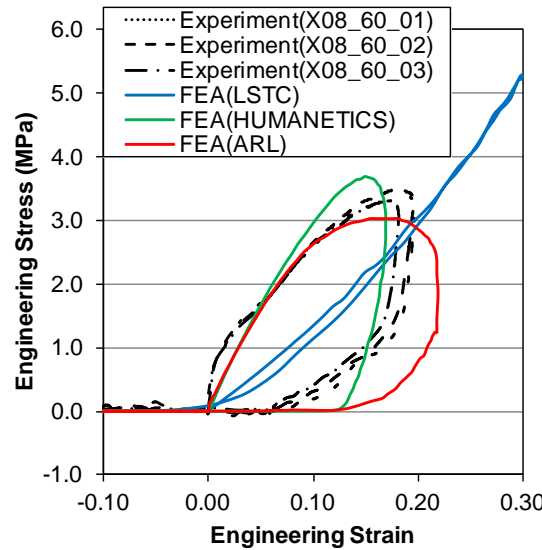


Fig. 22 Example of the engineering stress–strain curve comparison between experiments and FEAs, X08_60 ($\Delta T = 8$ msec, $\Delta V = 6.0$ m/s)

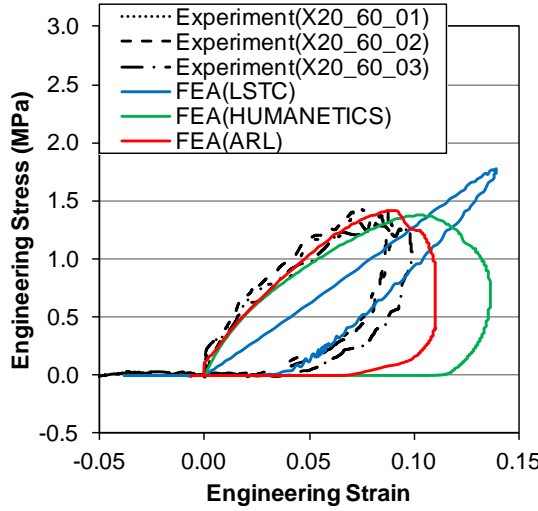


Fig. 23 Example of the engineering stress-strain curve comparison between experiments and FEAs, X20_60 ($\Delta T = 20$ msec, $\Delta V = 6.0$ m/s)

There are 2 cases for the formation of encircled areas in FEAs:

- 1) The material model assumes different material behaviors for the loading–unloading phases. However, the LSTC model is a viscoelastic material model and assumes the same behavior.
- 2) The material model assumes different material behaviors for the deformation speeds, and the speeds are different in the loading–unloading phases. This is the case for the LSTC model, and will be discussed in this section.

The shear relaxation modulus $G(t)$ is defined in the LSTC model as follows:

$$G(t) = G_{\infty} + (G_0 - G_{\infty}) e^{-\beta t}, \quad (2)$$

where G_{∞} is the infinite shear modulus, G_0 is the short-time shear modulus, and β is the decay constant. (G_{∞} , G_0 and β correspond to the parameters G0, GI, and BETA in Table 5, respectively.)

Therefore, the sensitivity of the material behavior against deformation speed is governed by β in an exponential manner. Judging from the formation of the encircled area in Fig. 23, the LSTC model was probably tailored for the loading with pulse longer than 20 msec. Consequently, the sensitivity in 4- and 8-msec-pulse loading is not enough to differentiate the loading–unloading curves according to their differences in the deformation speeds.

Although the Humanetics model has a similar description for the relaxation modulus as the LSTC model, the loading–unloading curves are differentiated. Moreover, the ARL model also differentiates the loading–unloading curves. Therefore, the Humanetics model and ARL model can be used for the evaluation of these loading–unloading events.

To clarify the accuracy of each material model, several metrics, E_0 , E_{Load} , and S_{ss} , are implemented as shown in Fig. 24. Each metric is defined below.

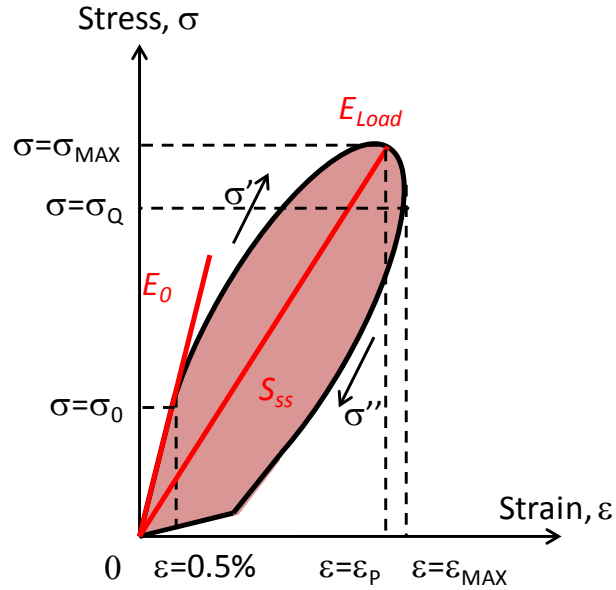


Fig. 24 Schematic of the stress–strain curve and metrics

The initial modulus E_0 represents the instantaneous material behavior and is defined as follows:

$$E_0 = \frac{\sigma_0 - 0}{0.005 - 0} \quad , \quad (5)$$

where σ_0 is the stress at 0.5% strain.

The loading modulus E_{Load} represents the overall loading behavior and is defined as follows:

$$E_{Load} = \frac{\sigma_{MAX} - 0}{\varepsilon_P - 0} \quad , \quad (6)$$

where σ_{MAX} is the maximum stress, and ε_P is the strain at the maximum stress point.

Encircled area S_{ss} represents the absorbed energy during the loading–unloading event and is defined as follows:

$$S_{ss} = \int_0^{\varepsilon_{MAX}} (\sigma' - \sigma'') d\varepsilon \quad , \quad (7)$$

where σ' is the stress in the loading curve, σ'' is the stress in the unloading curve, and ε_{MAX} is the maximum strain.

The errors of the FEA results versus the experimental results were calculated in these 3 metrics, as shown in Figs. 25–27. The errors of E_0 show that all 3 material models are not suitable for the prediction of instantaneous material behavior such as the rising edges of the experimental results (in Figs. 21 and 22).

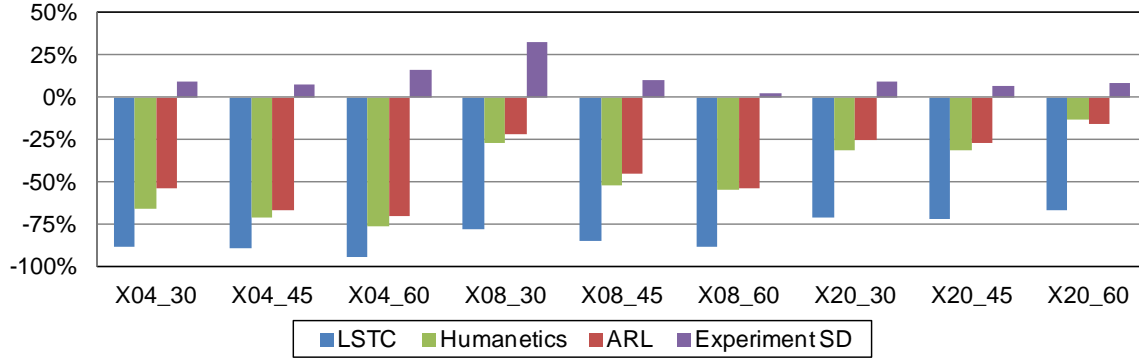


Fig. 25 Initial modulus errors of FEAs versus experimental test data

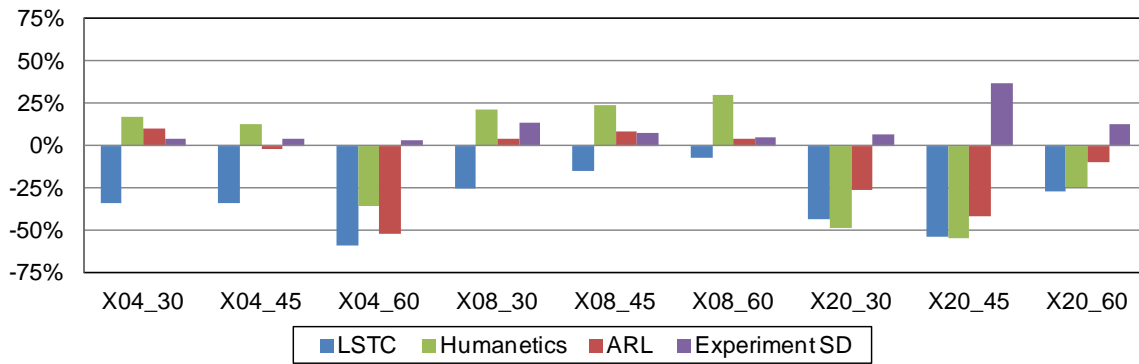


Fig. 26 Loading modulus errors of FEAs versus experimental test data

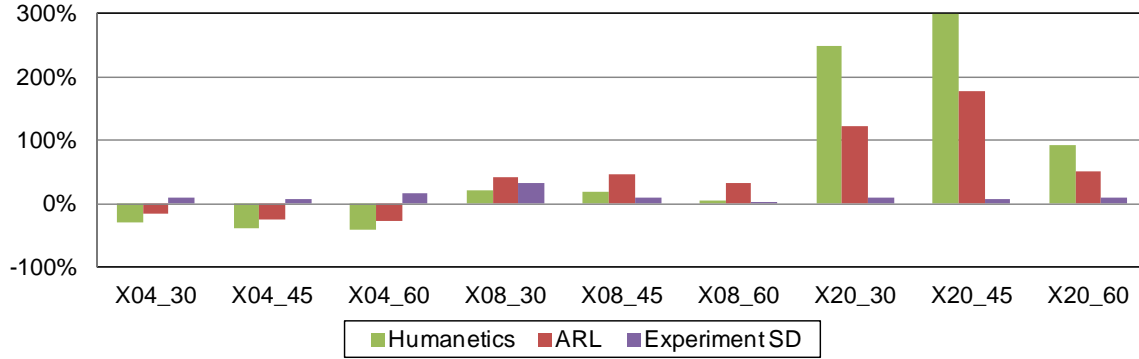


Fig. 27 Encircled area errors of FEAs versus experimental data. (LSTC model's errors are omitted due to poor differentiation in the loading-unloading curves.)

As shown in Fig. 26, the errors of E_{Load} are less than 25% in most of the FEA results of the ARL model in 4- and 8-msec-pulse loading. The only exception is the loading condition X04_60; this has the highest strain rate due to its short-duration, high-amplitude pulse. The strain rates of the experimental results in this loading condition are shown in Fig. 28. The maximum strain rate is approximately 150/s, and this is lower than the upper limit of the strain rate defined in the loading curves of the ARL model as shown in Fig. 6 (160/s). However, the strain rate in Fig. 28

is the averaged value over the whole specimen. Therefore, the partial strain rate probably exceeds the upper limit, and the ARL model tends to underestimate E_{Load} as E_0 in this loading condition. Moreover, this also leads to the underestimation of peak stress in the loading condition X04_60 as shown in Fig. 18. The FEA results of the Humanetics model and LSTC model also show small errors of E_{Load} in several loading conditions, but the errors are generally larger than those of the ARL model.

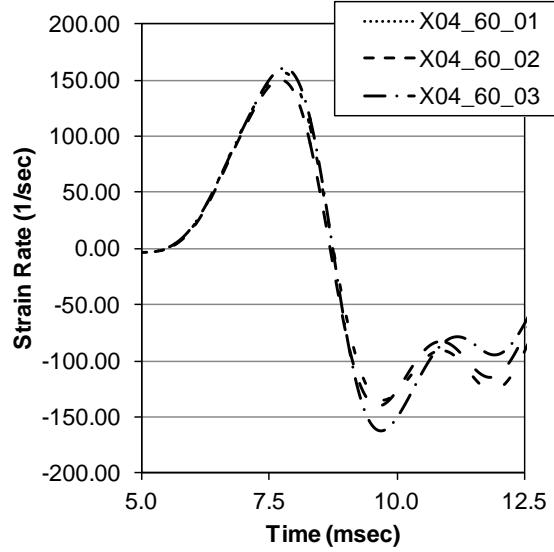


Fig. 28 Strain-rate histories of the specimen in the test condition, X04_60 ($\Delta T = 4$ msec, $\Delta V = 6.0$ m/s)

As to S_{ss} , the Humanetics model and ARL model show small errors for 4- and 8-msec-pulse loading. However, the deviation is larger than that of E_0 ; this should be noted in the evaluation of energy absorption on the FEA. In 20-msec-pulse loading, both models show large errors due to the overestimated strain in the unloading phase, which was discussed previously.

For these reasons, both the Humanetics model and ARL model can be used for the prediction of stress-strain curves in 4- and 8-msec-pulse loading, whereas the instantaneous material behaviors are not completely simulated. Both models also can be used for the prediction of energy absorption with larger errors. Moreover, the ARL model is superior to the Humanetics model, especially in the prediction of loading behavior.

4. Conclusions

In this study, we conducted component loading tests of butyl rubber and compared the results with those of FEAs to clarify the accuracy of the FE-material models. The Humanetics model and ARL model showed good accuracy in 4- and 8-msec-pulse loading for the prediction of stress history, strain history, stress-strain curve, impulse transfer, and energy absorption, while the LSTC model showed significant errors. Moreover, the ARL model is superior to the Humanetics model especially with its higher accuracy in the loading phase. Therefore, we conclude that the ARL model is to be used in the forthcoming FEA of the ATD's lower leg and the butyl-rubber floor mat. However, the current ARL model has two problems to be corrected:

- 1) The strain-rate dependency in the unloading phase is not completely installed in the models. This leads to the excessive recovery delay, especially in long-duration pulse loading.
- 2) The strain-rate dependency shown in Fig. 6 does not cover the partial, high strain-rate deformation. This leads to the excessively soft behavior in the loading phase and underestimation of the maximum stress.

Problem 2, in particular, affects the 4-msec-pulse loading that we frequently use in the evaluation of underbody blast-loading events. Therefore, the ARL model's improvement is strongly recommended.

5. References and Notes

1. Dougherty AL, Mohrle CR, Galarneau MR, Woodruff SI, Dye JL, Quinn KH. Battlefield extremity injuries in Operation Iraqi Freedom. *Injury*. 2009;40(7):772–777.
2. Belmont PJ, Schoenfeld AJ, Goodman G. Epidemiology of combat wounds in Operation Iraqi Freedom and Operation Enduring Freedom: orthopaedic burden of disease. *J Surg Orthop Adv*. 2010;19(1):2–7.
3. Eskridge SL, Macera CA, Galarneau MR, Holbrook TL, Woodruff SI, MacGregor AJ, Morton DJ, Shaffer RA. Injuries from combat explosions in Iraq: injury type, location, and severity. *Injury*. 2012;43(10):1678–1682.
4. Test methodology for protection of vehicle occupants against anti-vehicular landmine effects. NATO; 2007. Report No.: TR-HFM-090.
5. Golan G, Asaf Z, Ran E, Aizik F. Occupant legs survivability: an assessment through the utilization of field blast test methodology. Paper presented at: MABS22. Proceedings of the 22nd International Symposium on Military Aspects of Blast and Shock; 2012 Nov 4–9; Bourges, France.
6. Dong L, Zhu F, Jin X, Suresh M, Jiang B, Sevagan G, Cai Y, Li G, Yang KH. Blast effect on the lower extremities and its mitigation: a computational study. *J Mech Behav Biomed Mater*. 2013;28:111–124.
7. Livermore Software Technology Corp. National Crash Analysis Center, Hybrid III 50th Percentile Dummy, model LSTC.
8. Humanetics Innovative Solutions, Hybrid-III 50th Percentile Male Dummy, model v7.0.
9. Livermore Software Technology Corp. (US). LS-DYNA Keyword User's Manual—Volume III Material Models (Rev. 3372). 2013. p. 3–78, 79.
10. Effinger V. Modeling of viscoelastic materials with LS-DYNA. Paper presented at: 11th German LS-DYNA Forum. Proceedings of NAFEMS Conference; 2012 Oct 9–10; Ulm, Germany. p. 11,15,17.
11. Kolling S, DuBois PA, Benson DJ. A simplified rubber model with damage. Paper presented at: 4th German LS-DYNA Forum. Proceedings of NAFEMS Conference; Bamberg, Germany. 2005. p. B.II.1–10.

6. List of Symbols, Abbreviations, and Acronyms

ARL	US Army Research Laboratory
ATD	anthropomorphic test device
FE	Finite Element
FEA	Finite Element Analysis
IED	improvised explosive device
kN	kilonewton
LSTC	Livermore Software Technology Corporation
mm	millimeter
msec	millisecond
m/s	meters per second

1 DEFENSE TECH INFO CTR
(PDF) ATTN DTIC OCA

2 US ARMY RSRCH LABORATORY
(PDF) ATTN IMAL HRA MAIL & RECORDS MGMT
ATTN RDRL CIO LL TECHL LIB

1 US ARMY RSRCH LAB
(PDF) ATTN RDRL WMP F R KARGUS

INTENTIONALLY LEFT BLANK.